Journal of Water Process Engineering 53 (2023) 103601

Contents lists available at ScienceDirect

Journal of Water Process Engineering

journal homepage: www.elsevier.com/locate/jwpe

Carbon nitride-type polymers compounded with FeOCl to enhance the catalytic removal of antibiotics over a wide pH range: Performance and mechanism

Yu Jiang [a,b], Kang Mao [a,*], Jiabing Ran [b], Junxia Su [a], Guopei Huang [a], Xingli Zheng [a], Kuankuan Zhang [a], Hui Guan [a], Changying Yang [b], Hua Zhang [a]

[a] State Key Laboratory of Environmental Geochemistry, Institute of Geochemistry, Chinese Academy of Sciences, Guiyang 550081, China
[b] College of Biological and Pharmaceutical Sciences, China Three Gorges University, Yichang 443002, China

ARTICLE INFO

Keywords:
Carbon nitride-type polymers
FeOCl
Heterogeneous Fenton
Antibiotics
Degradation

ABSTRACT

The ubiquity of antibiotics challenges water treatment and public health. Herein, a novel heterogeneous Fenton system was constructed to remove antibiotics, and carbon nitride-type polymers compounded with FeOCl (CNPs/FeOCl) were used as catalysts. The efficiency for removal of tetracycline hydrochloride (TC-HCl) reached 100 % within 6 min ([TC-HCl] = 20 mg/L, [CNPs/FeOCl] = 0.2 g/L, [H_2O_2] = 0.3 mM, pH = 3.5), and the catalytic activity of CNPs/FeOCl was higher than those of FeOCl and CNPs alone. In particular, the TC-HCl degradation efficiencies over a wide pH range of 3 to 11 were nearly 100 % within 8 min. TC-HCl and its oxidation intermediates were degraded by the ·OH radicals produced from Fe^{2+}/Fe^{3+} induced degradation of H_2O_2, and small molecules (H_2O and CO_2) were eventually produced, which enabled antibiotic degradation through three possible pathways. Additional results showed that electrons promoted the cycling of Fe^{2+} and Fe^{3+} from the FeOCl, which enhanced the decomposition of H_2O_2 to produce more ·OH and improve the catalytic activity. Finally, the novel Fenton system catalyzed efficient degradations of antibiotics in natural water, providing a potential method for removal of antibiotics and other organic pollutants with CNPs/FeOCl.

1. Introduction

Widely used antibiotics inevitably flow into aqueous environments and are frequently detected in water columns [1–4], which poses major threats to human health and aquatic environments and creates conditions that facilitate the proliferation of antibiotic-resistant bacteria and antibiotic resistance genes [5]. The coexistence of antibiotics and antibiotic resistance genes increases the risks of creating new resistance genes and accelerates the spread of antibiotic-resistant bacteria in aquatic environments, which poses potentially lethal threats to the environment and public health [6–9]. For example, tetracycline, a typical antibiotic, is used to treat protozoan and bacterial infections in aquaculture, and due to improper handling of this antibiotic, tetracycline is subsequently discharged into the environment [10]. Consequently, effective measures are needed to address this challenge.

Fenton reactions are widely used for effective treatment of organic pollutants, and they use Fe^{2+} and H_2O_2 to generate ·OH under acidic conditions [11]. However, the Fenton reaction has certain limitations. One is that the divalent Fe^{2+} in the system is easily oxidized to Fe^{3+}, and the reaction rate of Fe^{3+} with H_2O_2 is very low; thus, methods are need to improve the Fe^{2+}/Fe^{3+} redox rate [12–14]. Another limitation is that the reaction must be performed under acidic conditions, which inevitably limits its application in neutral environments [15]. Furthermore, the entire system tends to produce iron sludge, which in turn pollutes the environment [6,16]. Due to these shortcomings, researchers have focused on developing catalysts that are catalytically active under acidic, neutral or even alkaline conditions [17]. In heterogeneous Fenton-like reactions, the Fe^{2+} in solution can be replaced with solid Fe-based catalysts, which mainly degrade organic pollutants with nonselective and highly active ·OH [18–20]. Typically, Fe_2O_3, Fe_3O_4, Mn—Fe compounds, and iron ore, among others, are used as heterogeneous iron-based catalysts [21–24]. Researchers have tried many techniques to improve the catalytic activities of the catalysts and have found that the introduction of transition metals or their oxides into the catalyst is an effective way to improve the catalytic activity [24–27].

In recent years, the two-dimensional catalytic material FeOCl has

* Corresponding author.
E-mail address: maokang@mail.gyig.ac.cn (K. Mao).

https://doi.org/10.1016/j.jwpe.2023.103601
Received 5 December 2022; Received in revised form 12 February 2023; Accepted 20 February 2023
Available online 2 March 2023

gradually received research attention [28–36]. Due to the weak interactions between the FeOCl layers, FeOCl can serve as an inorganic host molecule for intercalation reactions in which the guest molecules interact with, or adsorb onto, the FeOCl. FeOCl is an efficient catalyst with high catalytic activity due to its good photoelectric conversion properties, which provide abundant electrons to reduce 25 % of the existing Fe^{3+} to Fe^{2+}; thus, FeOCl has received widespread attention for use in Fenton reactions [30,36]. The standard reduction potential of FeOCl is relatively low, and the conversion of Fe^{3+} to Fe^{2+} is slow ($E^0(Fe^{3+}/Fe^{2+}) = 0.771$ eV), which inhibits its ability to activate H_2O_2; thus, the lack of Fe^{2+} regeneration makes practical applications difficult [37]. Therefore, improving the Fe^{2+}/Fe^{3+} redox cycle is a challenge that must be addressed, and researchers have conducted studies on this issue. For example, Sun et al. coated FeOCl on the surface of a polyvinylidene fluoride ultrafiltration membrane to modify the polyvinylidene fluoride and thus improve the antifouling performance and self-cleaning capability of the composite membrane, and these researchers used the composite membrane for degradation of bisphenol A [31]. Li et al. synthesized novel FeOCl-modified sludge-derived biochar composites and showed degradation efficiencies for rhodamine B of up to 99 % over a wide pH range [38]. Although the performance of FeOCl has been improved through these studies, its catalytic performance has not been significantly enhanced; therefore, problems associated with long degradation times and poor Fe^{2+}/Fe^{3+} redox cycling still need to be resolved.

Polymeric graphitic-phase carbon nitride (g-CN, g-C_3N_4) is a metal semiconductor, and the graphitic-phase carbon nitride is a conjugated polymer with tri-*s*-triazine repeat units and an sp^2-hybridized C—N backbone, which makes it of wide interest for use as a photocatalyst or carrier substrate in the field of catalysis [39,40]. g-CN, like graphene, is a two-dimensional layered structure that is nontoxic, inexpensive, thermally stable and easily dispersed, and it can be synthesized under acidic or alkaline conditions and is widely used as a carrier for environmental pollutant removal. g-CN has a high nitrogen content (theoretically higher than 60 %), and compared with other C—N materials, this structure more effectively disperses nanoparticles and enables rapid charge transfer to the active sites on the surface, increasing the generation of active substances for catalytic degradation of pollutants [41,42]. The downside is that g-CN alone cannot improve the catalytic conversion of activated H_2O_2 to ·OH. Therefore, modification with transition metal oxides or metal ion doping into the g-CN backbone are promising approaches. The electron-rich cavity in the g-CN backbone provides an ideal platform for trapping positive transition metal ions, and metal-containing catalytically active sites are available for multiphase catalytic processes [43–45]. Pi et al. synthesized $CoFe_2O_4$ via a hydrothermal method and g-CN as a carrier for the $CoFe_2O_4$-mediated degradation of levofloxacin in a peroxymonosulfate system and observed excellent catalytic activity [46]. Hak et al. prepared Ag/g-CN complexes by loading the precious metal Ag onto g-CN, and the Ag/g-CN complexes exhibited high catalytic activity for the degradation of bisphenol A [47]. However, the addition of g-CN to Fe to enhance the catalytic degradation of antibiotics has rarely been reported.

In addition, rapid electron transfer accelerates the operation of the Fe^{3+}/Fe^{2+} redox cycle that generates ·OH, which has high catalytic activity and therefore exhibits substantial potential to improve the Fe activity [48–51]. Thus, g-CN composites and FeOCl serve as complementary materials with great potential for addressing the individual limitations of FeOCl and g-CN and producing Fenton catalytic reagents.

Based on the mentioned above, we synthesized a novel carbon nitride-type polymer (CNPs) compounded with FeOCl to give the CNPs/FeOCl composite, improved the catalytic performance of the FeOCl and CNP catalysts and systematically evaluated the effects of experimental parameters, such as the mass ratio used for the catalyst synthesis, the pH of the pollutant, and the H_2O_2 dose, on the removal of antibiotics. TC-HCl was used as a typical antibiotic with which to test a new Fenton system and investigate the mechanism. The dual synergistic removal mechanism involving adsorption and degradation of the TC-HCl and the degradation pathway for TC-HCl were also explored and validated in natural water matrices. We expect that the CNPs/FeOCl composites will be useful heterogeneous Fenton catalysts and enable the removal of organic compounds such as antibiotics from aqueous environments.

2. Experimental section

For specific reagents and instruments, see the Supporting Text.

2.1. Preparation of the catalysts

2.1.1. Synthesis of CNPs

CNP nanosheets were prepared by using the solvothermal method with formamide as the precursor and nitrogen source [52]. 10 mL of formamide, 0.75 g of citric acid and 0.75 g of sodium acetate were stirred until the reaction was complete (40 min), which produced a prepolymer consisting of citric acid and formamide in a weakly alkaline environment. After thorough stirring, this solution was transferred to a 30 mL hydrothermal reaction kettle, heated in an oven to 230 °C, held at that temperature for 3 h and then cooled to room temperature to obtain a brown–black solution. The final mixture contained CNP nanosheets, and unreacted material was removed by centrifugation to give a nanosheet suspension. A large amount of ethanol was added to the solution to yield a brown–black precipitate, which had good water solubility. The precipitate was washed 3 times with ethanol and dried at 40 °C for 12 h to obtain the final product, which was labelled CNPs.

2.1.2. Synthesis of FeOCl

The preparation of FeOCl was carried out with a high-temperature sintering method. During the typical procedure, 0.5 g of $FeCl_3{\cdot}6H_2O$ was weighed and ground thoroughly in an agate mortar to obtain a yellow powder, which was subsequently transferred to a crucible, wrapped with aluminium foil, labelled and transferred to a muffle furnace to be heated to 250 °C at a heating rate of 2 °C/min, and the final temperature was maintained for 3 h. When the reaction was complete and the sample cooled to room temperature, it was removed, and the unreacted $FeCl_3{\cdot}6H_2O$ was rinsed out with a large amount of acetone until the solution ran clear. The FeOCl was then dried overnight in a vacuum drying oven at 60 °C for subsequent experiments.

2.1.3. Preparation of CNPs/FeOCl composites

The preparation of the CNPs/FeOCl composite involved reacting the synthesized CNPs with the precursor to FeOCl, as follows: 0.5 g of CNPs and 1.5 g of $FeCl_3{\cdot}6H_2O$ were weighed into a mortar and ground until well mixed, transferred to a crucible, wrapped with aluminium foil, and heated at a rate of 2 °C/min. After the reaction, the precipitate was washed several times with acetone by centrifugation until the supernatant was clear and transparent, and the precipitate was then transferred to a vacuum drying oven, heated at 60 °C and dried overnight for subsequent experiments; the resulting compound was labelled CNPs/FeOCl (1:3). Additionally, 1.5 g of the CNPs and 0.5 g of $FeCl_3{\cdot}6H_2O$ were weighed into a mortar and ground until well mixed, transferred to a crucible, wrapped with aluminium foil, and heated at a rate of 2 °C/min. The other steps were the same as above, and the resulting compound was labelled CNPs/FeOCl (3:1).

2.2. Antibiotic removal process

2.2.1. Antibiotic degradation process

The entire heterogeneous Fenton reaction was carried out in a 100 mL reaction flask for the TC-HCl degradation experiments. The initial pH of the TC-HCl solution was adjusted with 1 M HCl or NaOH. A 0.2 g/L catalyst solution was injected into the reaction flask containing the TC-HCl solution at room temperature, and 0.3 mM H_2O_2 was added at predetermined time intervals (2 min, 4 min, 6 min, 8 min, 10 min) to

initiate the reaction. A 1.6 mL sample was placed in the reaction flask, 300 μL of tert-butanol was added immediately to stop the reaction, and the solution was filtered through a 0.22 μm membrane for further analysis. Each group of experiments was performed three times, and the results were averaged. The samples obtained from the experiments were refrigerated at 4 °C for HPLC testing.

Pure adsorption experiments without the addition of H_2O_2 were carried out under the same conditions, and to evaluate the effect of CNPs/FeOCl adsorption on the removal of TC-HCl during the heterogeneous Fenton reaction, the same experiments were carried out as follows: the suspension was shaken in a constant temperature oscillator (25 °C, 150 rpm) for 24 h, and a certain volume of the solution was filtered to remove the solid catalyst. Each group of experiments was performed three times, and the results were averaged. After the experiments were conducted, the samples were refrigerated at 4 °C for HPLC analyses.

The adsorption/degradation experiments were performed under the same catalytic conditions; the adsorption experiments did not require the addition of H_2O_2, but the other conditions were the same as those of the degradation experiments.

To evaluate the feasibility of using the developed treatment method in complex matrices, actual water samples were used for validation. The water samples were collected from the Nanming River in Guiyang City, China and simulated TC-HCl degradation experiments were performed. Different concentrations of TC-HCl were added to the real water. The removal experiments were performed under the same catalytic conditions.

2.2.2. HPLC analysis process

The concentration of the TC-HCl solution was determined by high-performance liquid chromatography (Agilent-1260) with an ultraviolet detector using a reverse phase C18 column. The mobile phase for the TC-HCl consisted of 65 % sodium dihydrogen phosphate and 35 % acetonitrile, the elution flow rate was 1 mL/min, and the injection volume was 20 μL. The detection wavelength was 360 nm, and the column temperature was 25 °C. The mobile phase for amoxicillin (AM) consisted of 70 % potassium dihydrogen phosphate and 30 % methanol, the elution flow rate was 0.6 mL/min and the injection volume was 20 μL. The detection wavelength was 240 nm, and the column temperature was 30 °C; the mobile phase for sulfamethoxazole (SMX) consisted of 65 % H_2O (containing 0.1 % glacial acetic acid) and 35 % methanol, the elution flow rate was 0.8 mL/min and the injection volume was 20 μL; the detection wavelength was 270 nm and the column temperature was 30 °C.

2.3. Identification of intermediates by HPLC–MS

For liquid chromatography–mass spectrometry (HPLC–MS) run in the positive ionization mode, the following mobile phase was used: A-0.1 % formic acid aqueous solution and B-0.1 % formic acid-acetonitrile aqueous solution; for HPLC–MS run in the negative ionization mode, the following mobile phase was used: A-0.03 % ammonia aqueous solution and B-0.03 % ammonia-acetonitrile solution.

2.4. Procedure for ESR studies of ·OH during catalysis

To identify the catalytically active species, experiments designed to ·OH bursts were conducted by using 10 mM and 30 mM tert-butanol under the same catalytic conditions, and related experiments for superoxide radical bursts were conducted using p-benzoquinone (10 mM, 30 mM). Additionally, 5,5-dimethyl-1-pyrroline N-oxide (DMPO) was used as a spin trap to capture radicals in the ESR experiments for comparison. The solvent contained the TC-HCl substrate; the first group consisted of pure DMPO blank experiments without H_2O_2, the second group consisted of TC-HCl + H_2O_2 + DMPO (100 mM) experiments, and the third group consisted of TC-HCl + H_2O_2 + DMPO (100 mM) + CNPs/FeOCl.

3. Results and discussion

3.1. Characterization of the synthesized materials

Scheme 1 reflects the synthetic procedure for CNPs/FeOCl. As shown in Scheme 1, the CNPs were first prepared, and FeOCl was then loaded onto the CNPs to obtain the CNP composite.

To investigate the microstructures of the three compounds, the surface morphologies of FeOCl, CNPs, and CNPs/FeOCl were studied with scanning electron microscopy (SEM), transmission electron microscopy (TEM) and high-resolution transmission electron microscopy (HR-TEM), and the results are shown in Fig. 1. The SEM image of FeOCl and the CNPs showed lamellar and irregular ultrathin curved sheets, respectively (Fig. 1a, b). The SEM and TEM images of the CNPs/FeOCl composite are shown in Fig. 1c (1d-enlarged image) and e. FeOCl filled the porous lamellar structure of the CNPs, and the morphologies of the two materials changed after formation of the composite, which may be attributed to the fact that doping of the CNPs with the $FeCl_3{\cdot}6H_2O$ precursor during synthesis of the CNPs/FeOCl may have resulted in chemical changes during the high-temperature sintering process. Thus, the morphology of the composite did not reflect simple stacking of the two compounds used to form the composite. Fig. 1f also shows that both the CNPs and FeOCl were present in the CNPs/FeOCl composite. A crystal lattice band for FeOCl was also observed in the HR-TEM image for CNPs/FeOCl (Fig. 1g). Fig. 1h-n shows the elemental maps for Fe, O, Cl, N, and C, which were distributed on the CNPs/FeOCl composite. Among them, the presence of Fe, O, and Cl can be attributed to FeOCl, and the presence of C and N is attributed to the CNPs.

The purities and crystallinities of the prepared materials were characterized by X-ray diffraction (XRD). As shown in Fig. 2a, the (002) and (100) planes of the CNPs were indicated by the two diffraction peaks at 13.3° and 27.4° (JCPDS No. 87-1526) [53]. The 13.3° diffraction peak corresponded to structural stacking of tri-*s*-triazine units in the CNPs planar repeat unit, and the strong characteristic peak at 27.4° was caused by the graphite-like interlayer structural motifs [54]. This peak consisted of three diffraction peaks at 24.8°, 26.8°, and 28.2°, indicating the presence of different layered structures in the CNPs crystals, which was attributed to planar stacking and interlayer stacking of the aromatic chain segments [53]. All diffraction peaks for the pure FeOCl phase were matched with the standard card for FeOCl (JCPDS card No. 24-1005) [55–57]; for the CNPs/FeOCl composite, due to the low CNPs content, the diffraction peaks for the CNPs were not obvious in the XRD patterns of the CNPs/FeOCl composite, which may be attributed to wrapping of the CNPs with excess FeOCl, which masked the CNPs diffraction peak. Therefore, the main diffraction peak was that of FeOCl. In contrast, for CNPs/FeOCl (3:1), due to the low FeOCl content, the diffraction peak for FeOCl was not obvious in the XRD pattern of the CNPs/FeOCl (3:1) composite, which may be attributed to the excess CNPs that masked the diffraction peak for FeOCl; the pattern mainly showed the diffraction peak for the CNPs (Fig. S1). This is consistent with the results for CNPs/FeOCl (1:3).

To determine the functional groups and chemical bonds present in the catalyst, Fourier transform infrared (FT-IR) spectroscopy was used, as shown in Fig. 2b. The broad peak near 3387 cm^{-1} was assigned to the stretching mode of the O—H groups in the absorbed H_2O molecules on the surfaces of the three compounds, and the peak at 3466 cm^{-1} was attributed to the stretching vibrations of -NHx [58]. For FeOCl, the Fe—O group showed a clear absorption peak at 499.87 cm^{-1}, and a stretching vibration for Fe—Cl was indicated by a peak near 1625 cm^{-1} [59]. For the pure-phase CNPs compound, the absorption bands at 1394–1625 cm^{-1} corresponded to C═N stretching vibrations, and the stretching vibration of the C—N bond in the triazine units of the CNPs showed a peak near 798.3 cm^{-1}; the absorption edge at 483.6 cm^{-1} was related to the energy gap [60,61]. In the prepared CNPs/FeOCl system,

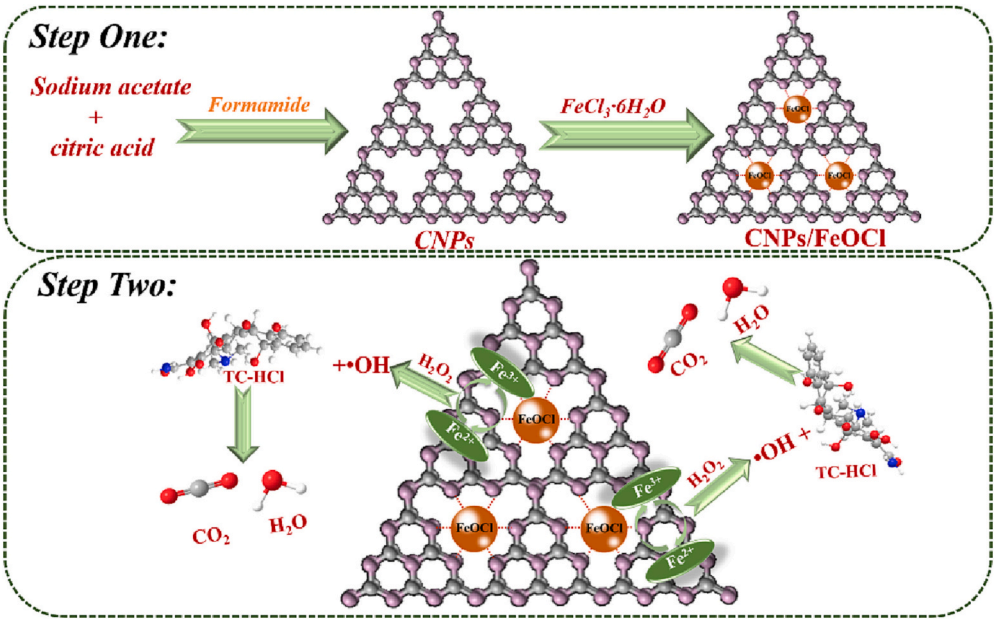

Scheme 1. Schematic of the synthetic procedure for CNPs/FeOCl and the TC-HCl degradation process.

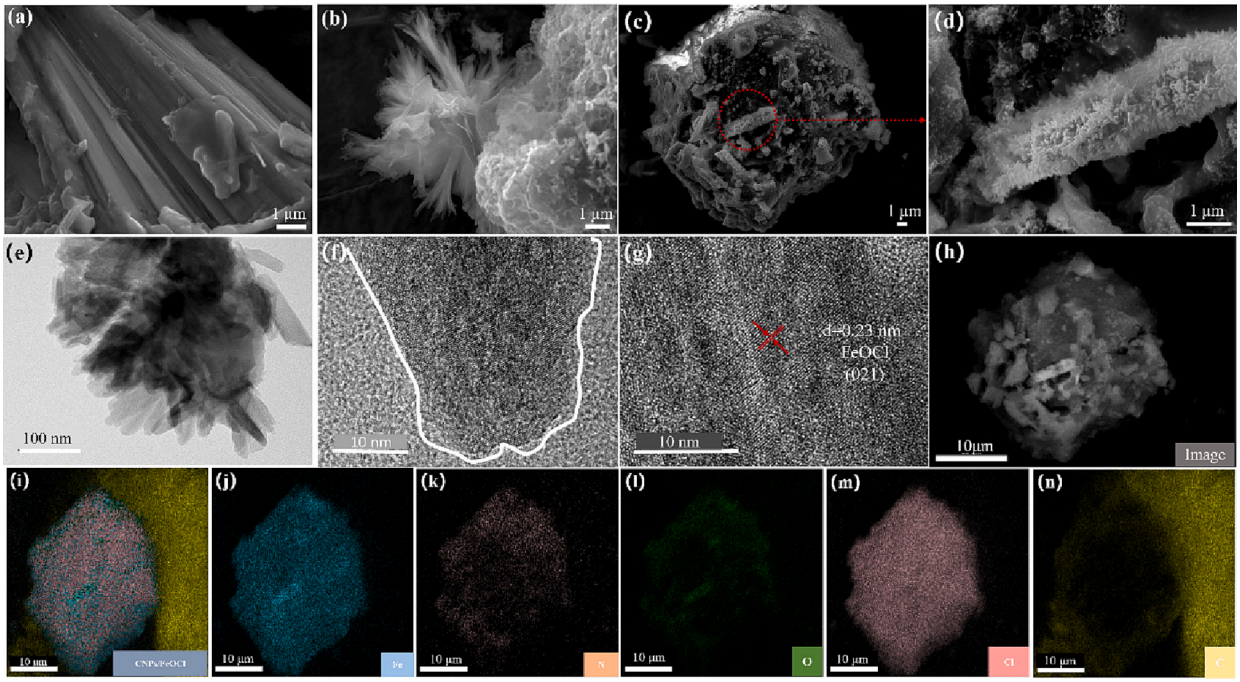

Fig. 1. Characterization of the synthesized materials. (a) SEM image of FeOCl; (b) SEM image of CNPs; (c) SEM image of CNPs/FeOCl; (d) SEM-based local enlargement of CNPs/FeOCl; (e) TEM image of CNPs/FeOCl; (f-g) HR-TEM images of CNPs/FeOCl. Elemental maps showing the distributions of the elements in the CNPs/FeOCl composite: (h) image of CNPs/FeOCl; (i) map of CNPs/FeOCl; distributions of (j) Fe, (k) N, (l) O, (m) Cl and (n) C.

the absorption band at 1625 cm^{-1} was assigned to C═O and -CH_2; the corresponding peaks for the doped FeOCl were not shifted, but the characteristic peaks in the complexes were weaker than those of the pure FeOCl. Therefore, these results proved that CNPs coexisted with FeOCl in the CNPs/FeOCl.

To investigate the chemical morphology of the CNPs/FeOCl composite, a detailed analysis was performed with X-ray photoelectron spectroscopy (XPS). The full spectrum in Fig. 2c shows the elements present in the composite. The presence of Fe, O, Cl, C, and N in the composite was confirmed. The spectrum in Fig. 2d showed the presence of C; the 284.8 eV, 288.2 eV, and 286.5 eV peaks corresponded to C—C, N-C═N, and C-O-C bonds in the CNPs, respectively [62–64]. A typical Cl 2p XPS spectrum is shown in Fig. 2e, and the characteristic peaks for Cl 2p binding energies of 197.6 eV and 199.3 eV corresponded to Fe—Cl bonds [65]. Fig. 2f shows the Fe 2p spectrum; the peaks at 711.2 eV and 725.17 eV corresponded to the binding energies of the $2p_{3/2}$ and $2p_{1/2}$ states of Fe^{3+}, respectively; the peaks at 710.26 eV and 723.45 eV were assigned to the $2p_{3/2}$ and $2p_{1/2}$ binding energies of Fe^{2+}, respectively, whereas the two peaks at 713.39 eV and 717.38 eV were satellite peaks [66–69]. In the N 1s spectrum of Fig. 4g, 398.6 eV and 399.7 eV are assigned to C-N═C bond and N (N-(C_3)) bond respectively [70]; 397.8 eV assigned to Fe—N [64,71]. Fig. 4h shows the spectrum of O 1s:

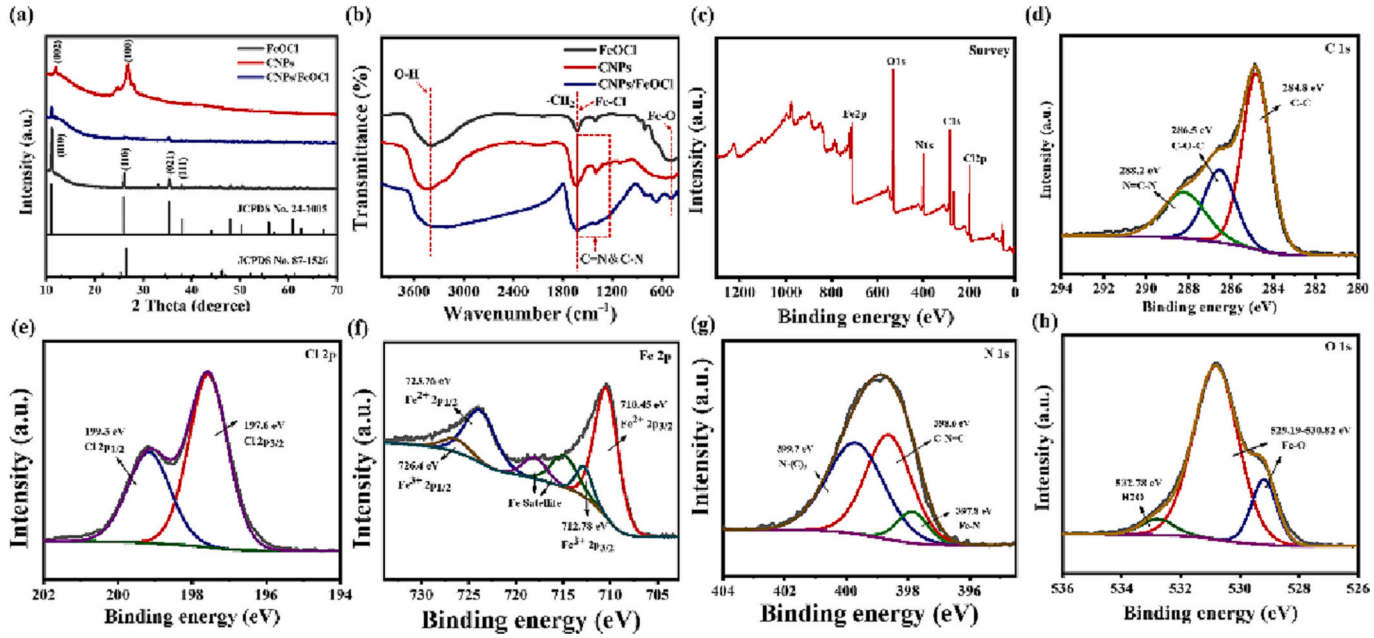

Fig. 2. (a) XRD patterns of FeOCl, CNPs, and CNPs/FeOCl; (b) FT-IR spectra of FeOCl, CNPs, and CNPS/FeOCl materials; (c-f) XPS spectra of CNPs/FeOCl after the reaction: (c) XPS survey spectrum, and (d) C 1s; (e) Cl 2p; (f) Fe 2p; (g) N 1s; (h) O1s XPS data.

529.19 eV–530.82 eV corresponds to the Fe—O bond phase matching of metal oxides in FeOCl lattice [56,67]; 532.78 eV is attributed to surface water molecules [72,73]; All of these findings confirmed the successful synthesis of the CNPs/FeOCl and the interactions between FeOCl and the CNPs. The other groups remained largely unchanged, indicating that these catalysts exhibited robust stability (Fig. S3).

Additionally, the surface areas and pore size distributions of the prepared materials were analysed with an automatic specific surface area and porosity analyser (BET). As shown in Fig. S2a and b, the prepared CNPs showed a type IV isotherm and a H_3 hysteresis loop, which indicated a mesoporous structure. The isotherms of FeOCl and CNPs/FeOCl were type I isotherms, which indicated microporous structures. The specific surface areas of the FeOCl, CNPs, and CNPs/FeOCl were 9.2854 m^2/g, 58.4287 m^2/g, and 9.1073 m^2/g, respectively. However, when FeOCl material was added to the CNPs, the specific surface area of the CNPs/FeOCl composite was equivalent to that of FeOCl. Surprisingly, the specific surface area of the CNPs/FeOCl composite was small, but tetracycline was adsorbed readily (Fig. 4a, b). These results showed why the formation of a microporous structure provides more active centres.

3.2. Evaluation of antibiotic degradation with CNPs/FeOCl

3.2.1. Effects of FeOCl and CNPs doping levels on CNPs/FeOCl

The removal of TC-HCl was evaluated with different systems. The Fe content had a significant effect on the removal of the contaminant via ·OH generation. As shown in Fig. 3a, the removal efficiency for TC-HCl reached 78.5 % within 10 min upon addition of H_2O_2 and FeOCl, and the removal rate for TC-HCl was only 27.0 % at 10 min upon addition of the pure CNPs. In contrast, the CNPs/FeOCl solution that contained a CNPs: FeOCl mass ratio of 1:3 showed significantly higher degradation activity for TC-HCl solutions compared with those seen for other mass ratios of the CNPs and FeOCl, and the removal efficiency for TC-HCl reached 100 % within only 8 min. Furthermore, when the amount of FeOCl exceeded the amount of CNPs, the XRD patterns for the complex showed a diffraction peak for FeOCl, but there was too little CNP to generate an observable diffraction peak, and the degradation rate of TC-HCl reached 100 % with the CNPs/FeOCl (1:3). In contrast, when there more CNPs than FeOCl, the XRD pattern of the complex mainly showed the diffraction peak for the CNPs (Fig. S1), and the rate of TC-HCl degradation was only 66 % with CNPs/FeOCl (3:1). This showed that the amount of FeOCl doping affected the catalytic performance of the

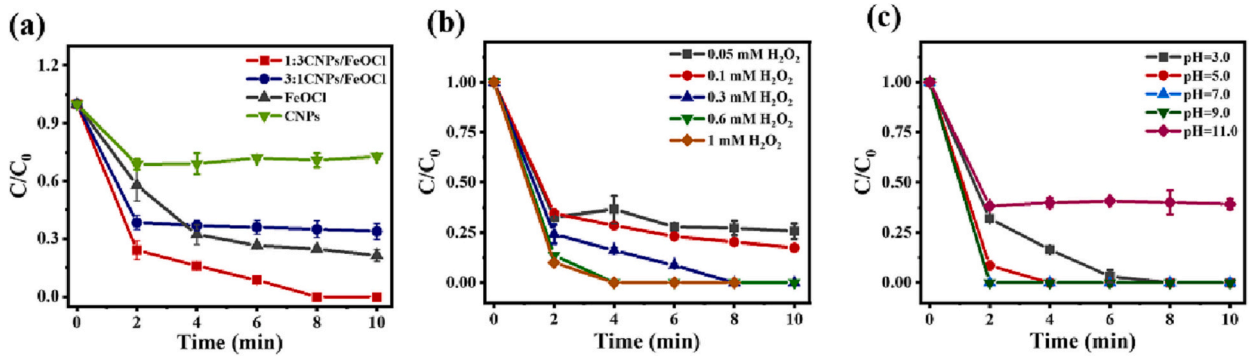

Fig. 3. (a) Effects of the FeOCl and CNPs proportions on TC degradation ($[TC\text{-}HCl]_{initial}$ = 20 ppm, [CNPs/FeOCl] = 0.2 g/L, $[H_2O_2]$ = 0.3 mM, and $[pH]_{initial}$ = 3.5); (b) Effect of H_2O_2 concentration on TC-HCl degradation ($[TC\text{-}HCl]_{initial}$ = 20 ppm, [CNPs/FeOCl] = 0.2 g/L, $[H_2O_2]$ = 0.3 mM, and $[pH]_{initial}$ = 3.5); (c) Effect of pH on TC-HCl removal by CNPs/FeOCl ($[TC\text{-}HCl]_{initial}$ = 20 ppm, [CNPs/FeOCl] = 0.2 g/L, $[H_2O_2]$ = 0.3 mM, and $[pH]_{initial}$ = 3.5).

composite, from the data of BET, when FeOCl was incorporated into the CNPs, the surface area of the CNPs/FeOCl was comparable to that of FeOCl; Fe constituted the active centre in the CNPs/FeOCl, and the combination of CNPs and FeOCl improved the adsorption performance of the composite so that the TC-HCl reached the catalyst surface faster. Therefore, preparation of the CNPs/FeOCl improved the catalytic performance beyond those of FeOCl and CNPs.

3.2.2. Effect of H_2O_2 dose on the degradation of TC-HCl

The concentration of H_2O_2 is also an important factor in a heterogeneous Fenton reaction. If the concentration of H_2O_2 is low, the amount of ·OH generated is insufficient to initiate the Fenton reaction successfully; if the concentration is too high, the H_2O_2 scavenges the ·OH generated in solution to reduce the catalytic efficiency, which waste reagents and increases the cost of catalysis. As a result, the effect of the H_2O_2 concentrations (0.05 mM, 0.1 mM, 0.3 mM, 0.6 mM, 1 mM) on TC-HCl degradation in the CNPs/FeOCl heterogeneous Fenton system was investigated. As shown in Fig. 3b, the TC-HCl removal efficiency was related to the H_2O_2 concentration and reached 100 % within 4 min when the H_2O_2 concentration was 1 mM, which was markedly higher than the TC-HCl removal efficiency seen when the H_2O_2 concentration was 0.05–0.6 mM.

3.2.3. TC-HCl degradation with different pH

The initial pH value is a key factor affecting the catalytic performance of the catalyst/H_2O_2 system. Since the Fenton reaction occurs over a narrow pH range (pH 2–3), which limits application in natural water samples, the influence of pH on the heterogeneous Fenton reaction has an effect on the nature of the catalyst, on the degradation of antibiotics, and on the decomposition of H_2O_2 [74–77]. To determine the role of H_2O_2 in the overall reaction system, the initial pH of the solution was varied (3.0, 5.0, 7.0, 9.0, 11.0) in the TC-HCl degradation experiments, as shown in Fig. 3c. The initial pH of the solution had a significant effect on TC-HCl removal, which was facilitated by pH of 3–9. In particular, in the pH range 7–9, the TC-HCl removal efficiency reached 100 % for a reaction of 2 min. When the pH was 11, the TC-HCl removal efficiency was 60 % with longer reactions times, except when CNPs/FeOCl adsorbed the TC-HCl, which indicated that H_2O_2 was more likely to produce ample ·OH under acidic, neutral, and weakly alkaline conditions. At low pH, the amine group of TC-HCl underwent protonation, and it was deprotonated at pH > 7. Thus, depending on the pH, the TC-HCl formed a protonated form or a deprotonated form; therefore, the pH played a crucial role in TC-HCl removal [78]. In terms of the reaction rate, the TC-HCl removal efficiency was as high as 100 % under neutral conditions with the optimal pH of 7.0, but the removal efficiency was severely affected by strongly acidic or basic conditions [79]. However, CNPs/FeOCl maintained excellent catalytic performance over a wide pH range. The results showed that CNPs/FeOCl effectively addressed the pH limitations of the homogeneous Fenton process without the introduction of light, which is preferred for use in real aqueous environments [80]. In addition, previous publications related to TC-HCl removal were investigated for comparison, as shown in Table 1. Compared with the other catalysts and their catalytic activities, the prepared catalyst required a shorter catalytic time and had a wider pH range (3−11) without the introduction of light, and it required less H_2O_2. Therefore, this catalyst could be applicable for antibiotic degradation.

3.2.4. Adsorption of TC-HCl by CNPs/FeOCl

During the catalytic experiments, the degradation process was accompanied by adsorption; thus, experiments on CNPs/FeOCl adsorption of TC-HCl were carried out. Fig. 4a demonstrates that the adsorption levels reached 105.26 mg/g. The adsorption capacity of CNPs/FeOCl at 1 h was high, and TC-HCl was completely adsorbed within 24 h (Fig. 4b). To demonstrate that TC-HCl adsorption was required in the degradation process, we used the same experimental conditions used for the degradation experiments and performed adsorption experiments without H_2O_2. As shown in Fig. 4c, the TC-HCl removal efficiency in the adsorption experiment was only 53.33 % after 10 min, whereas complete TC-HCl removal was achieved within 4 min in the degradation experiment run with H_2O_2, which indicated that adsorption and degradation occurred simultaneously and TC-HCl removal was accelerated by H_2O_2. Additionally, the heterogeneous Fenton system was shown to have practical value for degrading organic contaminants such as antibiotics.

3.2.5. Validation of antibiotic removal in actual water matrices

In actual water matrices, a variety of parameters may affect the performance of catalysts in many ways, such as by modulating the pH, capturing ·OH and influencing the efficiency of H_2O_2 decomposition. The effect of the natural water matrix on TC-HCl should not be neglected; therefore, to explore the effects of the water matrix on the

Table 1
Catalytic activities of different catalysts in Fenton reactions for TC-HCl degradation.

Catalyst category	[Catalyst] (g/L)	[TC-HCl] (mg/L)	[H_2O_2] (mM)	pH	Experimental result	Ref.
MoS_2/GDY	0.8	100	None	6.0	T = 40 min, Degradation efficiency = 92.15 %	[81]
Fe-doped $Bi_4O_5I_2$	0.75	20	17.4	3.0–9.0	T = 80 min Degradation efficiency≥90 %	[82]
Fe^0/CeO_2	0.1	100	100	5.8	T = 60 min Degradation efficiency = 91 %	[83]
Mn − CNH	0.2	20	0.6	5.8	T = 80 min Degradation efficiency = 100 %	[84]
$Cu_{0.8}Mn_{0.2}Fe_2O_4$	0.1	80	50	3	T = 30 min Degradation efficiency = 94.3 %	[85]
$MnFe_2O_4$@C-NH_2	1	30	29.4	3–9	T = 180 min Degradation efficiency = 95.5 %	[86]
CQDs/α-FeOOH	0.25	20	0.5	3.09	T = 60 min Degradation efficiency = 93 %	[87]
SOH-600	0.02–0.147	50	1.58	3.0	T = 60 min Degradation efficiency>90 %	[88]
$FeMo_3O_x$/g-C_3N_4	1.33	25	20	5.0	T = 60 min Degradation efficiency = 98 %	[89]
C@FONC	0.5	150	4.90	2,3	T = 120 min Degradation efficiency = 97 %	[90]
α-FeOOH/γ-Fe_2O_3	0.5	10	10	3.0	T = 60 min Degradation efficiency = 93 %	[91]
CNPs/FeOCl	0.2	20	0.3	7–9	T = 8 min Degradation efficiency = 100 %	This work

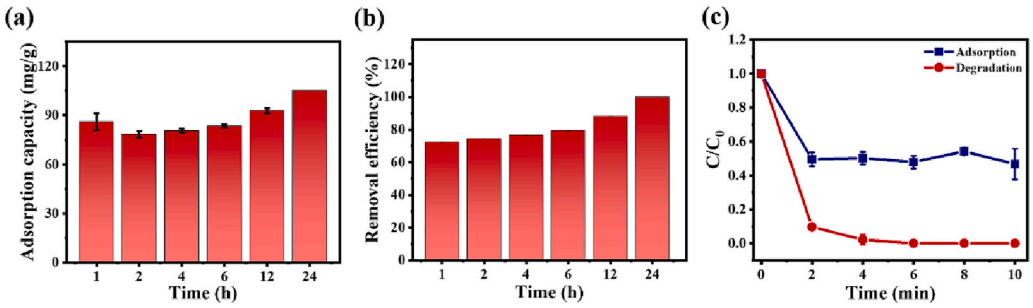

Fig. 4. (a) Adsorption of TC-HCl by CNPs/FeOCl (1:3) over 24 h; (b) Rate of TC-HCl removal by CNPs/FeOCl (1:3) over 24 h; (c) Comparison of adsorption/degradation experiments (experimental conditions: $[TC\text{-}HCl]_{initial}$ = 20 ppm, [CNPs/FeOCl (1:3)] = 0.2 g/L, $[H_2O_2]$ = 0.3 mM, and $[pH]_{initial}$ = 3.5).

degradation of TC-HCl, river water samples were collected. Before studying the impact of actual water samples on the degradation of TC-HCl, we carried out related analyses on the actual water samples and determined the conventional indicators of water quality, including pH, dissolved oxygen, dissolved organic carbon, water temperature and conductivity. In addition, we also tested the concentrations of antibiotics in the actual samples (Table S2). Fig. 5a demonstrates that surface water had no significant effect on TC-HCl degradation, and the removal rate still reached 95.9 %. Even when the concentration of TC-HCl was high (60 ppm), the CNPs/FeOCl composite showed strong adaptability in complex water matrices.

3.3. Degradation of other antibiotics

The above analyses showed that the CNPs/FeOCl composite was effective in degrading TC-HCl. To verify the general applicability of CNPs/FeOCl for use with other antibiotics, we chose two other common antibiotics, amoxicillin (AM) and sulfamethoxazole (SMX), as degradation targets. Under optimal conditions, the AM degradation efficiency of CNPs/FeOCl was higher than 90 % within 1 h (Fig. 5b). Fig. 5c shows the data for SMX degradation at different H_2O_2 concentrations, and the degradation efficiency of SMX was higher than 96 % when the H_2O_2 concentration was 10 mM. In summary, the CNPs/FeOCl showed high catalytic activity in degrading multiple antibiotics.

3.4. Degradation mechanism

3.4.1. Active species analysis

To gain insight into the degradation mechanisms, we investigated the TC-HCl degradation efficiency of CNPs/FeOCl with radical capture experiments (Fig. 6a). We chose different quenchers, including tert-butanol (TBA) and p-benzoquinone (PBQ), to quench the ·OH and superoxide radicals, such as $O_2\cdot^-$ and $HO_2\cdot$, respectively [92–94]. Fig. 6a shows that the TC-HCl degradation efficiencies were 64.95 % and 100 % after 10 min for degradation experiments run with and without TBA, respectively, which indicated that the addition of TBA inhibited the degradation reaction. The addition of PBQ did not inhibit the reaction rates in the degradation experiments, and the TC-HCl exhibited complete degradation, indicating that ·OH rather than $HO_2\cdot$ played a dominant role within the overall reaction.

To investigate the catalytic mechanisms of the major reactive species formed in the heterogeneous Fenton system by the composite, the species in the CNPs/FeOCl/H_2O_2 system, such as ·OH and superoxide radicals, were probed. Electron spin resonance (ESR) spectroscopy was applied with 5,5-dimethyl-1-pyrroline N-oxide (DMPO) used to trap the radicals [82]. As shown in Fig. 6b, various TC-HCl degradation experiments were conducted for comparison: the first group consisted of blank experiments with pure DMPO and without H_2O_2, the second group consisted of TC-HCl + H_2O_2 + DMPO (100 mM) experiments, and the

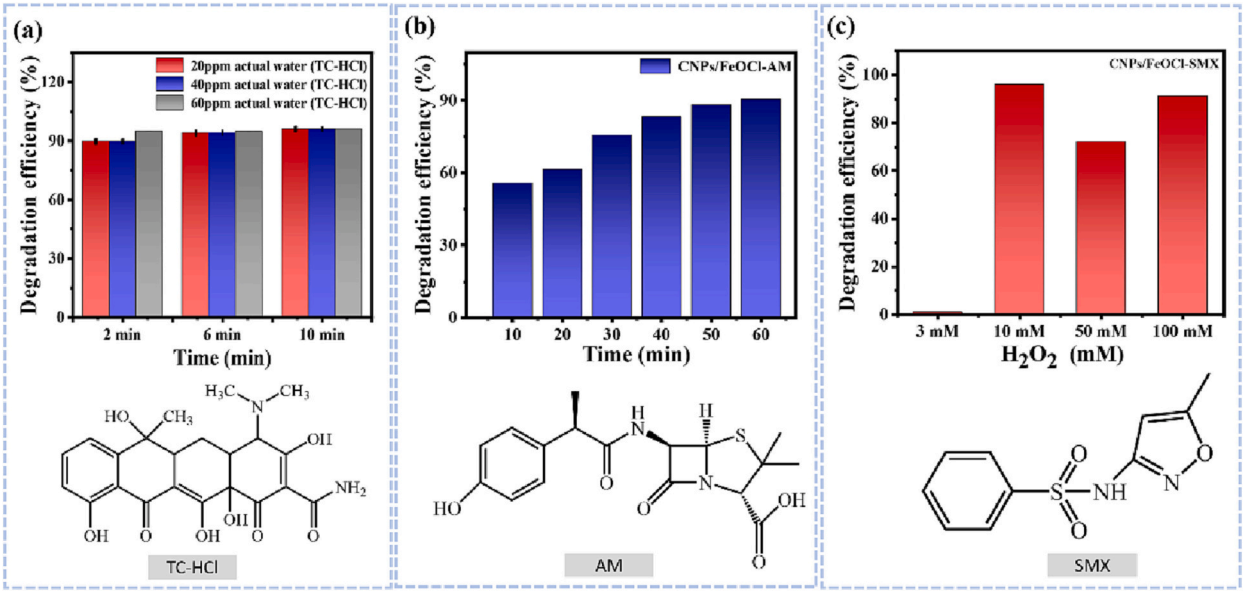

Fig. 5. (a) Effect of actual surface water samples (river water) on the removal of TC-HCl by CNPs/FeOCl composites (experimental conditions: [TC-HCl] = 20, 40, 60 ppm; $[H_2O_2]$ = 0.3 mM, [CNPs/FeOCl] = 0.2 g/L; pH = 3.5); (b) CNPs/FeOCl composite removal of amoxicillin (experimental conditions: [AM] = 20 ppm, $[H_2O_2]$ = 3 mM, [CNPs/FeOCl] = 0.2 g/L, pH = 3.5; (c) CNPs/FeOCl composite removal of sulfamethoxazole ([SMX] = 20 ppm, $[H_2O_2]$ = 3 mM, 10 mM, 50 mM, 100 mM, [CNPs/FeOCl] = 0.2 g/L, pH = 3.5).

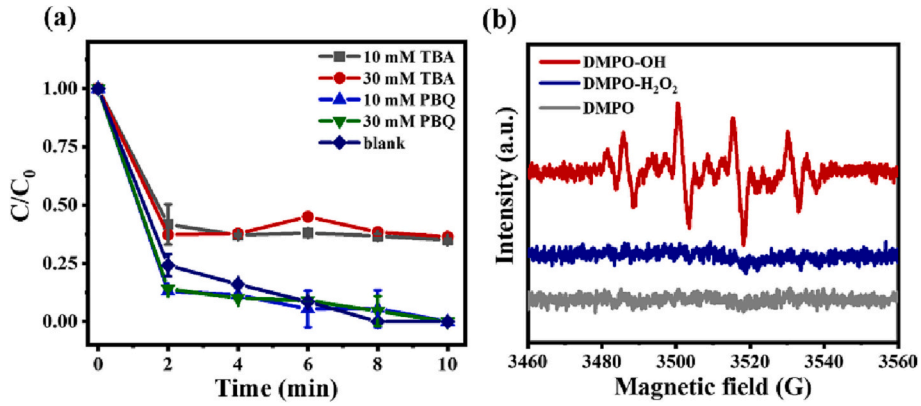

Fig. 6. (a) CNPs/FeOCl/H_2O_2 system studied with different scavengers (TBA = 10 mM, 30 mM; PBQ = 10 mM, 30 mM, and $[TC\text{-}HCl]_{initial}$ = 20 ppm, [CNPs/FeOCl] = 0.2 g/L, $[H_2O_2]$ = 0.3 mM, and $[pH]_{initial}$ = 3.5; (b) EPR identification of hydroxyl radicals ([DMPO] = 100 mM, $[TC\text{-}HCl]_{initial}$ = 20 ppm, [CNPs/FeOCl] = 0.2 g/L, $[H_2O_2]$ = 0.3 mM, and $[pH]_{initial}$ = 3.5).

third group consisted of TC-HCl + H_2O_2 + DMPO (100 mM) + CNPs/FeOCl experiments. As indicated in Fig. 6b, the typical quartet with the 1:2:2:1 intensity ratio exhibited by the stable DMPO-·OH adduct was observed in the experiments using TC-HCl + H_2O_2 + DMPO (100 mM) + CNPs/FeOCl; however, the other two sets of experiments did not show significant signals. The results are consistent with those of the radical burst experiment, which indicated that ·OH was the main active species for the removal of TC-HCl with CNPs/FeOCl/H_2O_2 by the heterogeneous Fenton system.

3.4.2. *Identification of possible degradation pathways*

The main intermediates of TC-HCl degradation were analysed by LC–MS in the positive ionization mode to understand the TC-HCl degradation pathway (Fig. 7). TC-HCl contains amine functional groups, double bonds, and phenolic groups susceptible to ·OH attack [95]. The TC-HCl intermediates formed via ·OH attack showed *m/z* values of 427, 491, and 417. New peaks with lower m/z values appeared with increasing degradation time, and their intensities increased significantly. These results showed that TC-HCl was converted to small organic molecules after 10 min of degradation, and additionally, organic macromolecules were no longer detectable by mass spectrometry. According to previous literature, the TC-HCl degradation process is complex and usually includes hydroxylation, decarboxylation, oxidation, dehydration, demethylation and double demethylation products [96–98]. According to the mass spectrometric results, there were three possible pathways for TC-HCl degradation (as seen in Fig. 7). In pathway I, ·OH, which is a nonselective radical, reacted with both aliphatic and aromatic fractions, and the reaction of ·OH with TC-HCl occurred at the aromatic ring and led to hydroxylation via ·OH attack to form an intermediate product for pathway II with an *m/z* value of 491 [90]. An intermediate with an m/z value of 293 was gradually degraded by aromatic ring cleavage, dehydroxylation, C—C bond breakage and demethylation occurring via carbon bond breakage and ring opening reactions; the intermediate with a m/z value of 261 was further degraded by aromatic ring and C—C bond cleavage. These results showed that the intermediates present were oxidized to carboxylic acids and eventually oxidized to small inorganic molecules. The intermediate product in pathway III with a m/z value of 417 was attacked by ·OH to generate a demethylated intermediate with an m/z value of 403, and the aliphatic ring was further degraded to form an intermediate product with an m/z value of 109 via reactions such as ring opening, dehydroxylation and C—C bond cleavage [99]. In addition, it has also been observed that the intermediate product with an m/z value of 417 can undergo amino acid deamination to form an intermediate with an m/z value of 402 [100,101], and this step is followed by deamidation, C—C single bond cleavage, and decarboxylation to form small organic molecules with m/z values of 151 and 107, respectively; the small organic molecules described above were eventually oxidized to CO_2 and H_2O. The intermediates formed throughout the reaction were monitored in real time by mass spectrometry (Table S1 and Fig. S4).

The cumulative results showed that CNPs/FeOCl/H_2O_2 effectively degraded TC-HCl. The ESR and radical burst results combined with data described above showed, as suggested in Scheme 1, that a heterogeneous Fenton reaction was feasible for TC-HCl degradation and that ·OH was the main active species. CNPs doping improved the charge transfer efficiency, and when $\equiv Fe^{3+}$ reacted with the H_2O_2, Fe^{3+} was immediately reduced to Fe^{2+}, and HO_2· and H^+ were produced (Eq. (1)). The additional $\equiv Fe^{2+}$ present in solution reacted with H_2O_2 to produce more of the active species ·OH and $\equiv Fe^{3+}$ (Eq. (2)), which in turn converted more Fe^{3+} to Fe^{2+}. Due to the ·OH radical attack, the structure of the pollutant was destroyed, small organic intermediates were produced, small inorganic molecules such as CO_2 or H_2O were ultimately generated, and ·OH was involved in the main pathway for TC-HCl degradation based on the ESR and degradation experiments.

$$\equiv Fe^{3+} + H_2O_2 \rightarrow \equiv Fe^{2+} + HO_2\cdot + H^+ \quad (1)$$

$$\equiv Fe^{2+} + H_2O_2 \rightarrow \equiv Fe^{3+} + \cdot OH + OH^- \quad (2)$$

$$e^- - + H_2O_2 \rightarrow \cdot OH + OH^- \quad (3)$$

$$\cdot OH + TC - HCl \rightarrow \text{Intermediate products} \quad (4)$$

$$\text{Intermediate products} + \cdot OH \rightarrow CO_2 + H_2O \quad (5)$$

4. Conclusion

In summary, the CNPs/FeOCl composite with a microporous structures comprising FeOCl and CNPs was successfully prepared via a simple microwave-assisted hydrothermal method and high-temperature sintering. The microporous composite material showed high catalytic activity as a Fenton catalyst for antibiotic removal with low H_2O_2 concentrations (0.6 mM), short reaction times (8 min) and a wide pH range (3–11). Furthermore, CNPs/FeOCl achieved 96.0 % removal of TC-HCl present with high concentrations in actual water samples. ESR spectroscopy and XPS showed that the combination of CNPs and FeOCl reduced FeOCl aggregation and enhanced interfacial electron transfer to enable Fe^{2+}/Fe^{3+} redox cycling. Moreover, several TC-HCl oxidation intermediates were identified, and three possible degradation pathways were elucidated. The fabricated CNPs/FeOCl composite, which showed excellent degradation performance with different antibiotics, provides a potentially efficient treatment strategy for the removal of antibiotics and other organic pollutants from aqueous environments over a wide pH

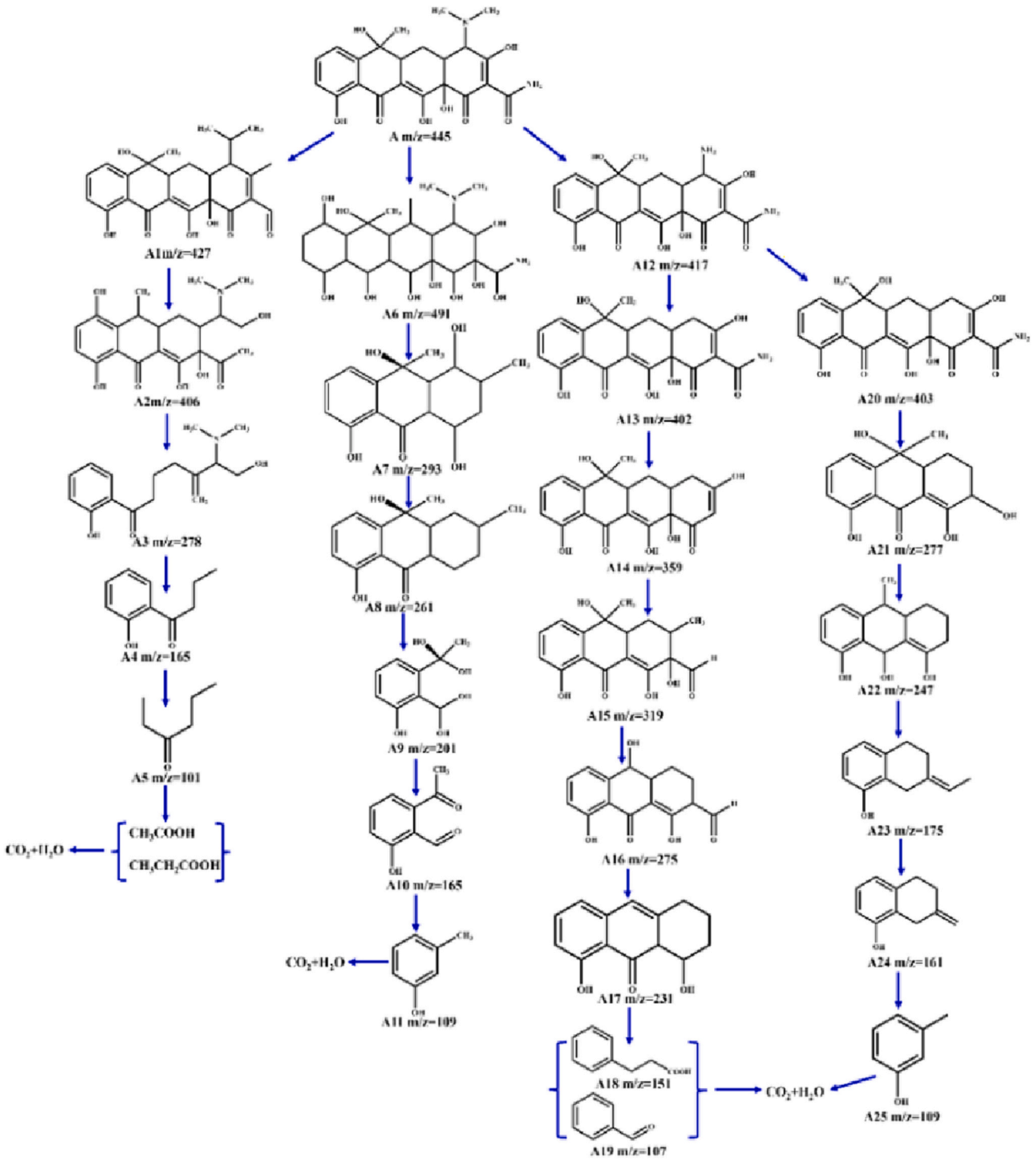

Fig. 7. Schematic diagram showing the possible degradation pathways for intermediate products formed in TC-HCl solution.

range.

Declaration of competing interest

The authors declare that they have no known competing financial interests or personal relationships that could have appeared to influence the work reported in this paper.

Data availability

Data will be made available on request.

Acknowledgements

This work was supported by the National Key Research and Development Program of China (2020YFC1807300), Youth Cross Team Project of CAS (JCTD-2021-17), and the Opening Funding of State Key Laboratory of Environmental Geochemistry (SKLEG2022209, 2022220).

Appendix A. Supplementary data

Supplementary data to this article can be found online at https://doi.org/10.1016/j.jwpe.2023.103601.

References

[1] M. Ahmadi, H.R. Motlagh, N. Jaafarzadeh, A. Mostoufi, R. Saeedi, G. Barzegar, S. Jorfi, Enhanced photocatalytic degradation of tetracycline and real pharmaceutical wastewater using MWCNT/TiO2 nano-composite, J. Environ. Manag. 186 (2017) 55–63.

[2] L. Prieto-Rodríguez, I. Oller, N. Klamerth, A. Agüera, E. Rodríguez, S. Malato, Application of solar AOPs and ozonation for elimination of micropollutants in municipal wastewater treatment plant effluents, Water Res. 47 (2013) 1521–1528.

[3] W. Yao, X. Wang, H. Yang, G. Yu, S. Deng, J. Huang, B. Wang, Y. Wang, Removal of pharmaceuticals from secondary effluents by an electro-peroxone process, Water Res. 88 (2016) 826–835.

[4] R. Zhang, Y. Yang, C.H. Huang, L. Zhao, P. Sun, Kinetics and modeling of sulfonamide antibiotic degradation in wastewater and human urine by UV/H2O2 and UV/PDS, Water Res. 103 (2016) 283–292.

[5] K. Ikehata, N. Jodeiri Naghashkar, M. Gamal El-Din, Degradation of aqueous pharmaceuticals by ozonation and advanced oxidation processes: a review, Ozone Sci. Eng. 28 (2006) 353–414.

[6] S.R. Shrivastava, P.S. Shrivastava, J. Ramasamy, World health organization releases global priority list of antibiotic-resistant bacteria to guide research, discovery, and development of new antibiotics, J. Med. Soc. 32 (2018) 76.

[7] K. Fent, A.A. Weston, D. Caminada, Ecotoxicology of human pharmaceuticals, Aquat. Toxicol. 76 (2006) 122–159.

[8] G. Na, W. Zhang, S. Zhou, H. Gao, Z. Lu, X. Wu, R. Li, L. Qiu, Y. Cai, Z. Yao, Sulfonamide antibiotics in the Northern Yellow Sea are related to resistant bacteria: implications for antibiotic resistance genes, Mar. Pollut. Bull. 84 (2014) 70–75.

[9] N. Zhang, X. Liu, R. Liu, T. Zhang, M. Li, Z. Zhang, Z. Qu, Z. Yuan, H. Yu, Influence of reclaimed water discharge on the dissemination and relationships of sulfonamide, sulfonamide resistance genes along the Chaobai River, Beijing, Front. Environ. Sci. Eng. 13 (2019) 1–12.

[10] R. Moreno-González, S. Rodriguez-Mozaz, M. Gros, D. Barceló, V. León, Seasonal distribution of pharmaceuticals in marine water and sediment from a mediterranean coastal lagoon (SE Spain), Environ. Res. 138 (2015) 326–344.

[11] B. Tryba, M. Piszcz, B. Grzmil, A. Pattek-Janczyk, A.W. Morawski, Photodecomposition of dyes on Fe-C-TiO2 photocatalysts under UV radiation supported by photo-Fenton process, J. Hazard. Mater. 162 (2009) 111–119.

[12] H. Sun, G. Xie, D. He, L. Zhang, Ascorbic acid promoted magnetite Fenton degradation of alachlor: mechanistic insights and kinetic modeling, Appl. Catal. B Environ. 267 (2020), 118383.

[13] Y. Sun, Z. Yang, P. Tian, Y. Sheng, J. Xu, Y.F. Han, Oxidative degradation of nitrobenzene by a Fenton-like reaction with Fe-Cu bimetallic catalysts, Appl. Catal. B Environ. 244 (2019) 1–10.

[14] Z. Jiang, L. Wang, J. Lei, Y. Liu, J. Zhang, Photo-Fenton degradation of phenol by CdS/rGO/Fe2+ at natural pH with in situ-generated H2O2, Appl. Catal. B Environ. 241 (2019) 367–374.

[15] B. Jain, A.K. Singh, H. Kim, E. Lichtfouse, V.K. Sharma, Treatment of organic pollutants by homogeneous and heterogeneous Fenton reaction processes, Environ. Chem. Lett. 16 (2018) 947–967.

[16] L.S.J. Jordá, M.B. Martín, E.O. Gómez, A.C. Reina, I.R. Sánchez, J.C. López, J. S. Pérez, Economic evaluation of the photo-Fenton process. Mineralization level and reaction time: the keys for increasing plant efficiency, J. Hazard. Mater. 186 (2011) 1924–1929.

[17] L. Clarizia, D. Russo, I. Di Somma, R. Marotta, R. Andreozzi, Homogeneous photo-Fenton processes at near neutral pH: a review, Appl. Catal. B Environ. 209 (2017) 358–371.

[18] J. Pignatello, Dark and photoassisted iron (3+)-catalyzed degradation of chlorophenoxy herbicides by hydrogen peroxide, Environ. Sci. Technol. 26 (1992) 944–951.

[19] Y. Zhu, R. Zhu, Y. Xi, J. Zhu, G. Zhu, H. He, Strategies for enhancing the heterogeneous Fenton catalytic reactivity: a review, Appl. Catal. B Environ. 255 (2019), 117739.

[20] J. Li, A.N. Pham, R. Dai, Z. Wang, T.D. Waite, Recent advances in Cu-Fenton systems for the treatment of industrial wastewaters: role of Cu complexes and Cu composites, J. Hazard. Mater. 392 (2020), 122261.

[21] B. Palanisamy, C. Babu, B. Sundaravel, S. Anandan, V. Murugesan, Sol–gel synthesis of mesoporous mixed Fe2O3/TiO2 photocatalyst: application for degradation of 4-chlorophenol, J. Hazard. Mater. 252 (2013) 233–242.

[22] J. Lu, Y. Zhou, Y. Zhou, Efficiently activate peroxymonosulfate by Fe3O4@MoS2 for rapid degradation of sulfonamides, Chem. Eng. J. 422 (2021), 130126.

[23] M. Wang, G. Fang, P. Liu, D. Zhou, C. Ma, D. Zhang, J. Zhan, Fe3O4@ β-CD nanocomposite as heterogeneous Fenton-like catalyst for enhanced degradation of 4-chlorophenol (4-CP), Appl. Catal. B Environ. 188 (2016) 113–122.

[24] Z. Wu, Y. Wang, Z. Xiong, Z. Ao, S. Pu, G. Yao, B. Lai, Core-shell magnetic Fe3O4@ Zn/Co-ZIFs to activate peroxymonosulfate for highly efficient degradation of carbamazepine, Appl. Catal. B Environ. 277 (2020), 119136.

[25] C. Hou, W. Chen, L. Fu, S. Zhang, C. Liang, Y. Wang, Facile synthesis of a Co/Fe bi-MOFs/CNF membrane nanocomposite and its application in the degradation of tetrabromobisphenol A, Carbohyd. Polym. 247 (2020), 116731.

[26] Z. Wu, Z. Tong, Y. Xie, H. Sun, X. Gong, P. Qin, Y. Liang, X. Yuan, D. Zou, L. Jiang, Efficient degradation of tetracycline by persulfate activation with Fe, Co and O co−doped g−C3N4: performance, mechanism and toxicity, Chem. Eng. J. 134732 (2022).

[27] L. Chen, X. Zuo, L. Zhou, Y. Huang, S. Yang, T. Cai, D. Ding, Efficient heterogeneous activation of peroxymonosulfate by facilely prepared Co/Fe bimetallic oxides: kinetics and mechanism, Chem. Eng. J. 345 (2018) 364–374.

[28] S. Vinoth, W.J. Ong, A. Pandikumar, Defect engineering of BiOX (X= Cl, Br, I) based photocatalysts for energy and environmental applications: current progress and future perspectives, Coordin. Chem. Rev. 464 (2022), 214541.

[29] J.C. Ahern, R. Fairchild, J.S. Thomas, J. Carr, H.H. Patterson, Characterization of BiOX compounds as photocatalysts for the degradation of pharmaceuticals in water, Appl. Catal. B Environ. 179 (2015) 229–238.

[30] C. Tan, Q. Xu, T. Sheng, X. Cui, Z. Wu, H. Gao, H. Li, Reactive oxygen species generation in FeOCl nanosheets activated peroxymonosulfate system: radicals and non-radical pathways, J. Hazard. Mater. 398 (2020), 123084.

[31] M. Sun, I. Zucker, D.M. Davenport, X. Zhou, J. Qu, M. Elimelech, Reactive, self-cleaning ultrafiltration membrane functionalized with iron oxychloride nanocatalysts, Environ. Sci. Technol. 52 (2018) 8674–8683.

[32] Z. Li, C. Guo, J. Lyu, Z. Hu, M. Ge, Tetracycline degradation by persulfate activated with magnetic Cu/CuFe2O4 composite: efficiency, stability, mechanism and degradation pathway, J. Hazard. Mater. 373 (2019) 85–96.

[33] Y. Ding, L. Zhu, N. Wang, H. Tang, Sulfate radicals induced degradation of tetrabromobisphenol A with nanoscaled magnetic CuFe2O4 as a heterogeneous catalyst of peroxymonosulfate, Appl. Catal. B Environ. 129 (2013) 153–162.

[34] X. Dong, B. Ren, Z. Sun, C. Li, X. Zhang, M. Kong, S. Zheng, D.D. Dionysiou, Monodispersed CuFe2O4 nanoparticles anchored on natural kaolinite as highly efficient peroxymonosulfate catalyst for bisphenol A degradation, Appl. Catal. B Environ. 253 (2019) 206–217.

[35] J. Yan, J. Peng, L. Lai, F. Ji, Y. Zhang, B. Lai, Q. Chen, G. Yao, X. Chen, L. Song, Technology, activation CuFe2O4 by hydroxylamine for oxidation of antibiotic sulfamethoxazole, Environ. Sci. Technol. 52 (2018) 14302–14310.

[36] X.j. Yang, X.m. Xu, J. Xu, Y.f. Han, Iron oxychloride (FeOCl): an efficient Fenton-like catalyst for producing hydroxyl radicals in degradation of organic contaminants, J. Am. Chem. Soc. 135 (2013) 16058–16061.

[37] Y. Feng, C. Liao, L. Kong, D. Wu, Y. Liu, P.H. Lee, K. Shih, Facile synthesis of highly reactive and stable Fe-doped g-C3N4 composites for peroxymonosulfate activation: a novel nonradical oxidation process, J. Hazard. Mater. 354 (2018) 63–71.

[38] M. Li, D. Xia, H. Xu, Z. Guan, D. Li, Iron oxychloride composite sludge-derived biochar for efficient activation of peroxymonosulfate to degrade organic pollutants in wastewater, J. Clean. Prod. 329 (2021), 129656.

[39] T. Ahmed, M. Ammar, A. Saleem, H.l. Zhang, H.b. Xu, Z-scheme 2D-m-BiVO4 networks decorated by a g-CN nanosheet heterostructured photocatalyst with an excellent response to visible light, RSC Adv. 10 (2020) 3192–3202.

[40] M. Aksoy, G. Yanalak, E. Aslan, İ.H. Patır, Ö. Metin, Visible light-driven hydrogen evolution by using mesoporous carbon nitride-metal ferrite (MFe2O4/mpg-CN; M: Mn, Fe, Co and Ni) nanocomposites as catalysts, Int. J. Hydrog.Energy 45 (2020) 16509–16518.

[41] S.M. Hossain, H. Park, H.J. Kang, J.S. Mun, L. Tijing, I. Rhee, J.H. Kim, Y.S. Jun, H.K. Shon, Facile synthesis and characterization of anatase TiO2/g-CN composites for enhanced photoactivity under UV–visible spectrum, Chemosphere 262 (2021), 128004.

[42] Z. Pan, G. Zhang, X. Wang, Polymeric carbon nitride/reduced graphene oxide/Fe2O3: all-solid-state Z-scheme system for photocatalytic overall water splitting, Angew. Chem. 131 (2019) 7176–7180.

[43] F. Dong, Z. Zhao, Y. Sun, Y. Zhang, S. Yan, Z. Wu, Technology, an advanced semimetal–organic Bi spheres–g-C3N4 nanohybrid with SPR-enhanced visible-light photocatalytic performance for NO purification, Environ. Sci. Technol. 49 (2015) 12432–12440.

[44] F. Raziq, J. He, J. Gan, M. Humayun, M.B. Faheem, A. Iqbal, A. Hayat, S. Fazal, J. Yi, Y. Zhao, Promoting visible-light photocatalytic activities for carbon nitride based 0D/2D/2D hybrid system: beyond the conventional 4-electron mechanism, Appl. Catal. B Environ. 270 (2020), 118870.

[45] X. Chen, J. Zhang, X. Fu, M. Antonietti, X. Wang, Fe-g-C3N4-catalyzed oxidation of benzene to phenol using hydrogen peroxide and visible light, J. Am. Chem. Soc. 131 (2009) 11658–11659.

[46] Y. Pi, H. Gao, Y. Cao, R. Cao, Y. Wang, J. Sun, Cobalt ferrite supported on carbon nitride matrix prepared using waste battery materials as a peroxymonosulfate activator for the degradation of levofloxacin hydrochloride, Chem. Eng. J. 379 (2020), 122377.

[47] C.H. Hak, L.C. Sim, K.H. Leong, P.F. Lim, Y.H. Chin, P. Saravanan, M/g-C3N4 (M= Ag, Au, and Pd) composite: synthesis via sunlight photodeposition and application towards the degradation of bisphenol A, Environ. Sci. Pollut. Res. 25 (2018) 25401–25412.

[48] V.H. Nguyen, M. Mousavi, J.B. Ghasemi, Q. Van Le, S.A. Delbari, M.S. Asl, M. Shokouhimehr, M. Mohammadi, Y. Azizian-Kalandaragh, A.S. Namini, In situ preparation of g-C3N4 nanosheet/FeOCl: achievement and promoted photocatalytic nitrogen fixation activity, J. Colloid Interf. Sci. 587 (2021) 538–549.

[49] S. Jiang, H. Zheng, X. Sun, M. Zhu, Y. Zhou, D. Wang, D. Zhang, L. Zhang, New and highly efficient ultra-thin g-C3N4/FeOCl nanocomposites as photo-Fenton

catalysts for pollutants degradation and antibacterial effect under visible light, Chemosphere 290 (2022), 133324.
[50] S. Asadzadeh-Khaneghah, A. Habibi-Yangjeh, D. Seifzadeh, H. Chand, V. Krishnan, E. Aspects, Visible-light-activated g-C3N4 nanosheet/carbon dot/FeOCl nanocomposites: photodegradation of dye pollutants and tetracycline hydrochloride, ColloidsSurf. A 617 (2021), 126424.
[51] S. Ahmadian-Fard-Fini, M. Salavati-Niasari, D. Ghanbari, Hydrothermal green synthesis of magnetic Fe3O4-carbon dots by lemon and grape fruit extracts and as a photoluminescence sensor for detecting of E. coli bacteria, Spectrochim. Acta A 203 (2018) 481–493.
[52] L.F. Gao, T. Wen, J.Y. Xu, X.P. Zhai, M. Zhao, G.W. Hu, P. Chen, Q. Wang, H. L. Zhang, Interfaces, iron-doped carbon nitride-type polymers as homogeneous organocatalysts for visible light-driven hydrogen evolution, ACS Appl. Mater. Interfaces 8 (2016) 617–624.
[53] Y.J. Yuan, Z. Shen, S. Wu, Y. Su, L. Pei, Z. Ji, M. Ding, W. Bai, Y. Chen, Z.T. Yu, Liquid exfoliation of g-C3N4 nanosheets to construct 2D–2D MoS2/g-C3N4 photocatalyst for enhanced photocatalytic H2 production activity, Appl. Catal. B Environ. 246 (2019) 120–128.
[54] B.w. Sun, H.y. Yu, Y.j. Yang, H.j. Li, C.y. Zhai, D.J. Qian, M. Chen, New complete assignment of X-ray powder diffraction patterns in graphitic carbon nitride using discrete Fourier transform and direct experimental evidence, Phys. Chem. Chem. Phys. 19 (2017) 26072–26084.
[55] M. Chen, H. Xu, Q. Wang, D. Li, D. Xia, Activation mechanism of sodium percarbonate by FeOCl under visible-light-enhanced catalytic oxidation, Chem. Phys. Lett. 706 (2018) 415–420.
[56] S. Sun, H. Yao, W. Fu, F. Liu, X. Wang, W. Zhang, Enhanced degradation of carbamazepine in FeOCl based photo-Fenton reaction, J. Environ. Chem. Eng. 9 (2021), 104501.
[57] B. Zhang, M. Chen, D. Li, H. Xu, D. Xia, Quantitative investigation into the enhancing utilization efficiency of H2O2 catalyzed by FeOCl under visible light, J. Photochem. Photobiol. A 386 (2020), 112072.
[58] S. Zinatloo-Ajabshir, M.S. Morassaei, M. Salavati-Niasari, Eco-friendly synthesis of Nd2Sn2O7–based nanostructure materials using grape juice as green fuel as photocatalyst for the degradation of erythrosine, Compos. Part B Eng. 167 (2019) 643–653.
[59] J. Zhang, G. Zhang, Q. Ji, H. Lan, J. Qu, H. Liu, Carbon nanodot-modified FeOCl for photo-assisted Fenton reaction featuring synergistic in-situ H2O2 production and activation, Appl. Catal. B Environ. 266 (2020), 118665.
[60] N.A. Mohamed, J. Safaei, A.F. Ismail, M.F.A.M. Jailani, M.N. Khalid, M.F.M. Noh, A. Aadenan, S.N.S. Nasir, J.S. Sagu, M.A.M. Teridi, The influences of post-annealing temperatures on fabrication graphitic carbon nitride,(g-C3N4) thin film, Appl. Surf. Sci. 489 (2019) 92–100.
[61] P. Niu, L. Zhang, G. Liu, H.M. Cheng, Graphene-like carbon nitride nanosheets for improved photocatalytic activities, Adv. Funct. Mater. 22 (2012) 4763–4770.
[62] H. Xu, Y. Song, Y. Song, J. Zhu, T. Zhu, C. Liu, D. Zhao, Q. Zhang, H. Li, Synthesis and characterization of gC3N4/Ag2CO3 with enhanced visible-light photocatalytic activity for the degradation of organic pollutants, RSC Adv. 4 (2014) 34539–34547.
[63] J. Yu, C. Xu, Z. Tian, Y. Lin, Z. Shi, Facilely synthesized N-doped carbon quantum dots with high fluorescent yield for sensing Fe 3+, New J. Chem. 40 (2016) 2083–2088.
[64] S. Asadzadeh-Khaneghah, A. Habibi-Yangjeh, D. Seifzadeh, Graphitic carbon nitride nanosheets coupled with carbon dots and BiOI nanoparticles: boosting visible-light-driven photocatalytic activity, J. Taiwan Inst. Chem. Eng. 87 (2018) 98–111.
[65] J. Xia, J. Di, H. Li, H. Xu, H. Li, S. Guo, Ionic liquid-induced strategy for carbon quantum dots/BiOX (X= Br, Cl) hybrid nanosheets with superior visible light-driven photocatalysis, Appl. Catal. B Environ. 181 (2016) 260–269.
[66] J. Zhao, M. Ji, J. Di, Y. Zhang, M. He, H. Li, J. Xia, Novel Z-scheme heterogeneous photo-Fenton-like g-C3N4/FeOCl for the pollutants degradation under visible light irradiation, J. Photochem. Photobiol. A 391 (2020), 112343.
[67] L. Jiang, L. Zhang, C. Cui, J. Zhang, G. Liu, J. Song, Efficient degradation of phenol using Sn4+ doped FeOCl as photo-Fenton catalyst, Mater. Lett. 240 (2019) 30–34.
[68] B. Adelekan, K. Abegunde, Heavy metals contamination of soil and groundwater at automobile mechanic villages in Ibadan, Nigeria, Int. J. Phys. Sci. 6 (2011) 1045–1058.
[69] Y. Chen, Y. Liu, L. Zhang, P. Xie, Z. Wang, A. Zhou, Z. Fang, J. Ma, Efficient degradation of imipramine by iron oxychloride-activated peroxymonosulfate process, J. Hazard. Mater. 353 (2018) 18–25.
[70] Y. Bao, K. Chen, AgCl/Ag/g-C3N4 hybrid composites: preparation, visible light-driven photocatalytic activity and mechanism, Nano-Micro Lett. 8 (2016) 182–192.
[71] J. Ma, Q. Yang, Y. Wen, W. Liu, Fe-g-C3N4/graphitized mesoporous carbon composite as an effective Fenton-like catalyst in a wide pH range, Appl. Catal. B Environ. 201 (2017) 232–240.
[72] J. Zhang, G. Liu, S. Liu, 2D/2D FeOCl/graphite oxide heterojunction with enhanced catalytic performance as a photo-Fenton catalyst, New J. Chem. 42 (2018) 6896–6902.
[73] Y. Wang, H. Zhang, Y. Zhu, Z. Dai, H. Bao, Y. Wei, W. Cai, Au-NP-decorated crystalline FeOCl nanosheet: facile synthesis by laser ablation in liquid and its exclusive gas sensing response to HCl at room temperature, Adv. Mater. Interfaces 3 (2016), 1500801.
[74] Y. Liu, X. He, Y. Fu, D.D. Dionysiou, Degradation kinetics and mechanism of oxytetracycline by hydroxyl radical-based advanced oxidation processes, Chem. Eng. J. 284 (2016) 1317–1327.
[75] S. Navalon, R. Martin, M. Alvaro, H. Garcia, Gold on diamond nanoparticles as a highly efficient Fenton catalyst, Angew. Chem. 49 (2010) 8403–8407.
[76] R.G. Zepp, B.C. Faust, J. Hoigne, Technology, hydroxyl radical formation in aqueous reactions (pH 3–8) of iron (II) with hydrogen peroxide: the photo-Fenton reaction, Environ. Sci. Technol. 26 (1992) 313–319.
[77] E. Brillas, S. Garcia-Segura, Benchmarking recent advances and innovative technology approaches of Fenton, photo-Fenton, electro-Fenton, and related processes: a review on the relevance of phenol as model molecule, Sep. Purif. Technol. 237 (2020), 116337.
[78] Y.H. Huang, Y.F. Huang, C.i. Huang, C.Y. Chen, Efficient decolorization of azo dye Reactive Black B involving aromatic fragment degradation in buffered Co2+/PMS oxidative processes with a ppb level dosage of Co2+-catalyst, J. Hazard. Mater. 170 (2009) 1110–1118.
[79] X. Li, Y. Huang, C. Li, J. Shen, Y. Deng, Degradation of pCNB by Fenton like process using α-FeOOH, Chem. Eng. J. 260 (2015) 28–36.
[80] R. Liu, Y. Xu, B. Chen, Self-assembled nano-FeO (OH)/reduced graphene oxide aerogel as a reusable catalyst for photo-Fenton degradation of phenolic organics, Environ. Sci. 52 (2018) 7043–7053.
[81] B. Huo, F. Meng, J. Yang, Y. Wang, J. Qi, W. Ma, Z. Wang, J. Wang, Z. Wang, High efficiently piezocatalysis degradation of tetracycline by few-layered MoS2/GDY: mechanism and toxicity evaluation, Chem. Eng. J. 436 (2022), 135173.
[82] C. Zhu, Y. Wang, L. Qiu, Y. Liu, H. Li, Y. Yu, J. Li, W. Yang, 3D hierarchical Fe-doped Bi4O5I2 microflowers as an efficient Fenton photocatalyst for tetracycline degradation over a wide pH range, Sep. Purif. Technol. 120878 (2022).
[83] N. Zhang, J. Chen, Z. Fang, E.P. Tsang, Ceria accelerated nanoscale zerovalent iron assisted heterogenous Fenton oxidation of tetracycline, Chem. Eng. J. 369 (2019) 588–599.
[84] Y. Mao, P. Wang, D. Zhang, Y. Xia, Y. Li, W. Zeng, S. Zhan, J.C. Crittenden, Accelerating FeIII-Aqua complex reduction in an efficient solid–liquid-interfacial Fenton reaction over the Mn–CNH co-catalyst at near-neutral pH, Environ. Sci. Technol. 55 (2021) 13326–13334.
[85] Y. Sun, J. Zhou, D. Liu, X. Li, H. Liang, Enhanced catalytic performance of Cu-doped MnFe2O4 magnetic ferrites: tetracycline hydrochloride attacked by superoxide radicals efficiently in a strong alkaline environment, Chemosphere 297 (2022), 134154.
[86] H. Qin, H. Cheng, H. Li, Y. Wang, Degradation of ofloxacin, amoxicillin and tetracycline antibiotics using magnetic core–shell MnFe2O4@C-NH2 as a heterogeneous Fenton catalyst, Chem. Eng. J. 396 (2020), 125304.
[87] S. Huang, Q. Zhang, P. Liu, S. Ma, B. Xie, K. Yang, Y. Zhao, Novel up-conversion carbon quantum dots/α-FeOOH nanohybrids eliminate tetracycline and its related drug resistance in visible-light responsive Fenton system, Appl. Catal. B Environ. 263 (2020), 118336.
[88] H. Wang, T. Chen, D. Chen, X. Zou, M. Li, F. Huang, F. Sun, C. Wang, D. Shu, H. Liu, Sulfurized oolitic hematite as a heterogeneous Fenton-like catalyst for tetracycline antibiotic degradation, Appl. Catal. B Environ. 260 (2020), 118203.
[89] Y. Liu, X. Wang, Q. Sun, M. Yuan, Z. Sun, S. Xia, J. Zhao, Enhanced visible light photo-Fenton-like degradation of tetracyclines by expanded perlite supported FeMo3Ox/g-C3N4 floating Z-scheme catalyst, J. Hazard. Mater. 424 (2022), 127387.
[90] J. Zhou, F. Ma, H. Guo, D. Su, Activate hydrogen peroxide for efficient tetracycline degradation via a facile assembled carbon-based composite: synergism of powdered activated carbon and ferroferric oxide nanocatalyst, Appl. Catal. B Environ. 269 (2020), 118784.
[91] Y. Ma, B. Wang, Q. Wang, S. Xing, Facile synthesis of α-FeOOH/γ-Fe2O3 by a pH gradient method and the role of γ-Fe2O3 in H2O2 activation under visible light irradiation, Chem. Eng. J. 354 (2018) 75–84.
[92] S. Asadzadeh-Khaneghah, A. Habibi-Yangjeh, K. Nakata, Decoration of carbon dots over hydrogen peroxide treated graphitic carbon nitride: exceptional photocatalytic performance in removal of different contaminants under visible light, J. Photochem. Photobiol. A 374 (2019) 161–172.
[93] M. Mousavi, A. Habibi-Yangjeh, Magnetically recoverable highly efficient visible-light-active g-C3N4/Fe3O4/Ag2WO4/AgBr nanocomposites for photocatalytic degradations of environmental pollutants, Adv. Powder Technol. 29 (2018) 94–105.
[94] M. Ji, Y. Liu, J. Di, R. Chen, Z. Chen, J. Xia, H. Li, N-CQDs accelerating surface charge transfer of Bi4O5I2 hollow nanotubes with broad spectrum photocatalytic activity, Environ. Chem. Lett. 237 (2018) 1033–1043.
[95] J. Wang, D. Zhi, H. Zhou, X. He, D. Zhang, Evaluating tetracycline degradation pathway and intermediate toxicity during the electrochemical oxidation over a Ti/Ti4O7 anode, Water Res. 137 (2018) 324–334.
[96] Q. Zhang, L. Jiang, J. Wang, Y. Zhu, Y. Pu, W. Dai, Photocatalytic degradation of tetracycline antibiotics using three-dimensional network structure perylene diimide supramolecular organic photocatalyst under visible-light irradiation, Appl. Catal. B Environ. 277 (2020), 119122.
[97] X. Li, K. Cui, Z. Guo, T. Yang, Y. Cao, Y. Xiang, H. Chen, M. Xi, Heterogeneous Fenton-like degradation of tetracyclines using porous magnetic chitosan microspheres as an efficient catalyst compared with two preparation methods, Chem. Eng. J. 379 (2020), 122324.
[98] C. Lai, F. Huang, G. Zeng, D. Huang, L. Qin, M. Cheng, C. Zhang, B. Li, H. Yi, S. Liu, Fabrication of novel magnetic MnFe2O4/bio-char composite and heterogeneous photo-Fenton degradation of tetracycline in near neutral pH, Chemosphere 224 (2019) 910–921.
[99] Z. Shi, Y. Zhang, X. Shen, G. Duoerkun, B. Zhu, L. Zhang, M. Li, Z. Chen, Fabrication of g-C3N4/BiOBr heterojunctions on carbon fibers as weaveable

photocatalyst for degrading tetracycline hydrochloride under visible light, Chem. Eng. J. 386 (2020), 124010.

[100] S. Li, C. Wang, M. Cai, Y. Liu, K. Dong, J. Zhang, Designing oxygen vacancy mediated bismuth molybdate (Bi2MoO6)/N-rich carbon nitride (C3N5) S-scheme heterojunctions for boosted photocatalytic removal of tetracycline antibiotic and Cr (VI): intermediate toxicity and mechanism insight, J. Colloid Interf. Sci. 624 (2022) 219–232.

[101] Y. Zhou, C. Zhang, D. Huang, W. Wang, Y. Zhai, Q. Liang, Y. Yang, S. Tian, H. Luo, D. Qin, Structure defined 2D Mo2C/2Dg-C3N4 Van der Waals heterojunction: oriented charge flow in-plane and separation within the interface to collectively promote photocatalytic degradation of pharmaceutical and personal care products, Appl. Catal. B Environ. 301 (2022), 120749.